The Astrophysical Journal Letters, 864:L13 (7pp), 2018 September 1 https://doi.org/10.3847/2041-8213/aada17

On the Impact of Helium Content on the RR Lyrae Distance Scale

M. Marconi[1], G. Bono[2,3], A. Pietrinferni[4], V. F. Braga[5,6], M. Castellani[3], and R. F. Stellingwerf[7]
[1] INAF—Osservatorio Astronomico di Capodimonte, Via Moiariello 16, I-80131 Napoli, Italy; marcella.marconi@oacn.inaf.it
[2] Dipartimento di Fisica, Università di Roma Tor Vergata, Via della Ricerca Scientifica 1, I-00133 Roma, Italy; giuseppe.bono@roma2.infn.it
[3] INAF—Osservatorio Astronomico di Roma, Via Frascati 33, I-00078 Monte Porzio Catone, Italy; marco.castellani@oa-roma.inaf.it
[4] INAF—Osservatorio Astronomico d'Abruzzo, Via M. Maggini SNC, I-64100 Teramo, Italy; adriano@oa-teramo.inaf.it
[5] Instituto Milenio de Astrofisica, Santiago, Chile; vittorio.braga@roma2.infn.it
[6] Departamento de Fisica, Facultad de Ciencias Exactas, Universidad Andres Bello, Fernandez Concha 700, Las Condes, Santiago, Chile
[7] Stellingwerf Consulting, 11033 Mathis Mountain Road SE, Huntsville, AL 35803, USA; rfs@swcp.com
Received 2018 April 5; revised 2018 August 10; accepted 2018 August 11; published 2018 August 29

Abstract

We constructed new sets of He-enhanced ($Y = 0.30$, $Y = 0.40$) nonlinear, time-dependent convective hydrodynamical models of RR Lyrae (RRL) stars covering a broad range in metal abundances ($Z = 0.0001$–0.02). The increase in He content from the canonical value ($Y = 0.245$) to $Y = 0.30$–0.40 causes a simultaneous increase in stellar luminosity and in pulsation period. To investigate the dependence of the RRL distance scale on the He abundance, we computed new optical (*RI*) and near-infrared (*JHK*) Period–luminosity–metallicity–helium relations. Interestingly enough, the increase in He content causes a minimal change in the coefficients of both period and metallicity terms, since canonical and He-enhanced models obey similar PLZ relations. On the contrary, the classical *B*- and *V*-band mean magnitude metallicity relations and the *R*-band PLZ relation display a significant dependence on the He content. The He-enhanced models are, at fixed metal content, 0.2–0.5 mag brighter than canonical ones. This variation is only marginally affected by evolutionary effects. The quoted distance diagnostics once calibrated with trigonometric parallaxes (*Gaia*) will provide the opportunity to estimate the He content of field and cluster RRLs. Moreover, the use of either spectroscopic or photometric metal abundances will pave the way to new empirical constraints on the universality of the helium-to-metal enrichment ratio in old ($t \gtrsim 10$ Gyr) stellar tracers.

Key words: stars: evolution – stars: horizontal-branch – stars: oscillations – stars: variables: RR Lyrae

1. Introduction

During the past century, RR Lyrae (RRL) stars have played a crucial role as standard candles and tracers of old stellar populations (Marconi et al. 2015; Madore et al. 2017; Neeley et al. 2017). They are old ($t \gtrsim 10$ Gyr), low-mass radial variables in their central helium burning phase and are observed in the Milky Way (Vivas & Zinn 2006; Drake et al. 2013; Zinn et al. 2014; Pietrukowicz et al. 2015), Local Group (Soszyński et al. 2010; Fiorentino et al. 2012; Coppola et al. 2015), and Local Volume galaxies (Da Costa et al. 2010; Sarajedini et al. 2012).

RRLs are used as standard candles since they obey a relation between absolute visual magnitude and iron abundance (Caputo et al. 2000; Cacciari & Clementini 2003; Di Criscienzo et al. 2004). This relation, whose linearity has also been questioned in the literature (Caputo et al. 2000; Catelan et al. 2004; Di Criscienzo et al. 2004), suffers from significant intrinsic errors and systematics. RRLs do not obey a period–luminosity (PL) relation in the optical bands, but thanks to the characteristic behavior of near-infrared (NIR) bolometric corrections (Bono et al. 2001, 2003), they obey a PL relation in the NIR regime (Longmore et al. 1990; Braga et al. 2015; Coppola et al. 2015).

The advantages of these relations are the small dependence on reddening and evolutionary effects (Bono et al. 2003) and a milder dependence on metallicity when compared with *B*, *V* magnitudes. Theory and observations indicate that more metal-rich RRLs are fainter than metal-poor ones, but we still lack firm constraints on the coefficient of the metallicity term in the NIR PL relations (Bono et al. 2003; Catelan et al. 2004; Dall'Ora et al. 2004; Sollima et al. 2006; Marconi et al. 2015).

Optical and NIR Period–Wesenheit (PW) relations are solid diagnostics for determining individual RRL distances, but rely on the assumed reddening law (Di Criscienzo et al. 2004; Braga et al. 2015; Coppola et al. 2015; Marconi et al. 2015). These relations are reddening free by construction (Madore 1982; Riess et al. 2012; Ripepi et al. 2012; Fiorentino et al. 2013; Inno et al. 2013) and include a color term. This means that they mimic a period–luminosity–color relation, tracing the position of each variable inside the instability strip (IS). These are the reasons why PW relations have been widely adopted to trace the 3D structure of highly reddened clusters in the Galactic Bulge (Soszyński et al. 2014; Pietrukowicz et al. 2015).

The main motivations for the current investigations are the following.

(a) The helium-to-metal enrichment ratio ($\Delta Y/\Delta Z = 1.4$, with a primordial He abundance of 0.245) adopted in evolutionary (Pietrinferni et al. 2006) and pulsation (Marconi et al. 2015) calculations is still affected by large uncertainties. RRLs are good laboratories for estimating the He content (Caputo 1998). To provide a new spin on the determination of this parameter, we are investigating new pulsation observables together with spectroscopic measurements of the metal content for field and cluster RRLs.

(b) Using the ΔS method, Walker & Terndrup (1991) found that Bulge RRLs approach solar metallicity. This finding was recently supported by Chadid et al. (2017) using

high-resolution spectra, since they found several RRLs at solar chemical compositions. This means a metallicity regime in which RRL pulsation properties are more prone to helium effects (Bono et al. 1995b; Marconi et al. 2011).

(c) The RRL distance scale is going to play a crucial role to constrain possible systematics affecting primary distance indicators (Beaton et al. 2016). Sizable samples of RRLs have already been identified in Local Group galaxies (Monelli et al. 2017) and beyond (Da Costa et al. 2010). However, we still lack firm theoretical and empirical constraints on the $\Delta Y/\Delta Z$ ratio in extragalactic systems.

To overcome the limitations of the current theoretical framework, we computed new sets of pulsation models with the same metal abundances ($Z = 0.0001$–0.02) adopted in Marconi et al. (2015) but that are helium enriched[8] ($Y = 0.30$ and $Y = 0.40$; M. Marconi et al. 2018, in preparation).

2. Impact of Helium-enhanced Models on RRL Distances

Following the same prescriptions as in Marconi et al. (2015) for both evolutionary and pulsation computations, and the same seven metal abundances, new sets of He-enhanced RRL models were computed with $Y = 0.30$ and $Y = 0.40$. The entire set of horizontal branch (HB) models (Pietrinferni et al. 2006) are available in the BaSTI database.[9] They were computed, for each assumed chemical composition, using a fixed core mass and envelope chemical profile and evolving a progenitor from the pre-main sequence to the tip of the red giant branch with an age of ∼13 Gyr. For each chemical composition, the mass distribution of HB models ranges from the mass of the progenitors (coolest HB models) down to a total mass of the order of $0.5\,M_{\odot}$ (hottest HB models).

The evolutionary phases off the zero-age horizontal branch (ZAHB) have been extended either to the onset of thermal pulses, for more massive models, or until the luminosity of the model (along the white dwarf cooling sequence) becomes fainter than $\log(L/L_{\odot}) \sim -2.5$ for less massive structures. The α-elements were enhanced with respect to the Grevesse et al. (1993) [10] solar metal distribution by variable factors (see Table 1 in Pietrinferni et al. 2006). The overall enhancement—[α/Fe]—is equal to 0.4 dex.

Figure 1 shows the behavior of HB models in the Hertzsprung–Russell diagram for three assumptions on the helium and on the metal content. In each panel, the black solid line shows the location of the ZAHB, the dashed black line corresponds to a central helium exhaustion at 90% level, and the long-dashed line denotes the complete exhaustion. Note that the ZAHB becomes dotted for masses higher than the progenitor one, artificially included to populate the IS. The blue and the red vertical lines display the predicted blue and red edge of the IS. The red solid lines show selected evolutionary models of HB structures populating the RRL IS. They range from $0.76\,M_{\odot}$ to $0.80\,M_{\odot}$ for $Z = 0.0001$, $Y = 0.245$ (top left panel), and from 0.520 to $0.525\,M_{\odot}$ for $Z = 0.0164$, $Y = 0.400$ (bottom right panel). Evolutionary prescriptions plotted in Figure 1 bring forward some relevant properties concerning He-enhanced stellar structures worth being discussed.

(i) *HB morphology*: He-enhanced stellar populations, at fixed metal content and cluster age, are characterized by smaller stellar masses at the main-sequence turnoff. This means smaller stellar masses at the tip of the red giant branch and an HB morphology dominated by hot and extreme stars. The HB luminosity function is, therefore, dominated by stars that are hotter than the blue edge of the IS. These stellar systems can still produce RRLs, since hot HB stars cross the IS just before or soon after the AGB phase (post-early-AGB; Greggio & Renzini 1990; D'Cruz et al. 1996). This means that the red HB and the IS are poorly populated (see the middle and right panels of Figure 1).

(ii) *Evolutionary timescale inside the IS*: The evolutionary time spent by a canonical, metal-poor ($Z = 0.0001$, $Y = 0.245$) stellar structure ($M = 0.84\,M_{\odot}$) inside the IS during the central He burning phases is $t_{\rm HB} \sim 67$ Myr. This time decreases by at least a factor of two when moving to He-enhanced models with $Y = 0.30$ ($M = 0.82\,M_{\odot}$, $t_{\rm HB} \sim 32$ Myr) and by a factor of six for models with $Y = 0.40$ ($M = 0.82\,M_{\odot}$, $t_{\rm HB} \sim 11$ Myr). The quoted trend marginally changes with the metal content, and indeed, canonical models at solar iron abundance ($Z = 0.0198$, $Y = 0.273$, $M = 0.5450\,M_{\odot}$) spend an evolutionary time of $t_{\rm HB} \sim 29$ Myr inside the IS ,and this time decreases down to $t_{\rm HB} \sim 15$ Myr for $Y = 0.30$ ($M = 0.5425\,M_{\odot}$) and to $t_{\rm HB} \sim 5$ Myr for $Y = 0.40$ ($M = 0.5230\,M_{\odot}$). The consequence of this difference is that the number of RRLs produced by He-enhanced stellar populations is at least one order of magnitude smaller than canonical ones. The reader is referred to M. Marconi et al. (2018, in preparation) for more details.

(iii) *Evolutionary timescale to approach the IS*: The increase in helium content causes, at fixed metallicity, a steady decrease in the evolutionary timescale required to approach the IS. This effect is more severe in the metal-poor regime (see the top panels in Figure 1) where the ZAHB for He-enhanced models located inside the IS is populated by stellar structures that are significantly younger than typical RRLs. Canonical stellar structures with $Z = 0.0001$ and $Y = 0.245$ evolve from the zero-age main sequence (ZAMS) to the ZAHB portion located inside the IS on a timescale of ∼12.5 Gyr (Valcarce et al. 2012). A He-enhanced stellar structure with $Z = 0.0001$ and $Y = 0.30$ evolves from the ZAMS to the IS in ∼8.5 Gyr, while for $Y = 0.40$ the same timescale becomes of the order of ∼4.5 Gyr. A similar trend is also present among stellar structures with $Z = 0.0006$ and $Y = 0.40$, since they approach the portion of the ZAHB located inside the IS with ages younger than ∼8.5 Gyr. On the other hand, for $Z = 0.001$ and $Y = 0.40$ the ZAHB stellar structures located inside the IS have ages that are only marginally younger (11–12 Gyr) than canonical ones. Note that the current empirical evidence indicates that RRL stars have *only* been identified in stellar populations older than 10 Gyr (Dékány et al. 2018).

[8] Metal (Z) and helium (Y) abundances by mass fraction.

[9] http://www.oa-teramo.inaf.it/BASTI/

[10] Note that new solar abundances by Asplund et al. (2009) provide lower CNO abundances when compared with Grevesse et al. (1993). The difference in metal distributions mainly causes a difference in the zero-point. The impact on the HB mass–luminosity relation is within the different luminosity levels adopted, at fixed mass and chemical composition, to construct pulsation models.

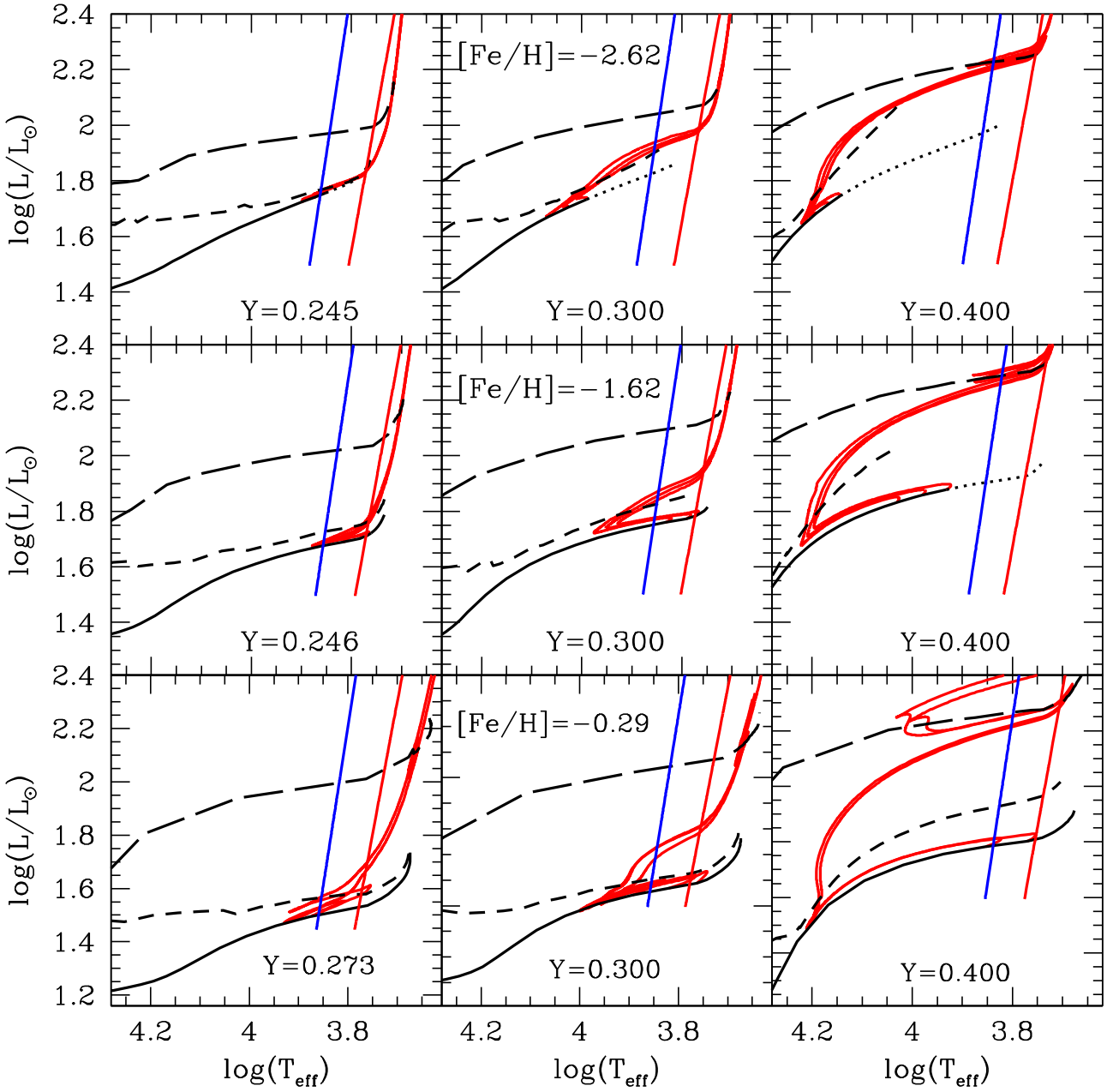

Figure 1. Hertzsprung–Russell diagrams of low-mass helium burning stellar structures. Top—from left to right evolutionary prescriptions for a metal-poor iron abundance (see labeled value) and three different helium contents. The solid lines display the zero-age horizontal branch (ZAHB), while the dotted lines show the extension to younger progenitors until the crossing of the RRL IS. The dashed and the long-dashed lines display the 90% and the 100% central helium exhaustion. The red solid lines display three HB evolutionary models covering the mass range typical of RRLs located close to the blue edge, to the middle of the IS, and to the red edge of the IS. The blue and the red, almost vertical, lines show the blue and the red edge of the predicted RRL IS. Middle—same as the top, but for a metal-intermediate chemical composition. Bottom—same as the top, but for a more metal-rich chemical composition.

On the basis of the quoted evolutionary prescriptions, we computed a set of pulsation models, for each iron and helium abundance, accounting for two values of the stellar mass and three different luminosity levels. The reasons for this choice were already discussed in Marconi et al. (2015). Here, we only give the highlights: (1) the ZAHB mass and luminosity level as based on the adopted evolutionary models; (2) the ZAHB mass and a luminosity level 0.1 dex brighter than the ZAHB luminosity; (3) a stellar mass 10% smaller than the ZAHB value and a luminosity level 0.2 dex brighter than the ZAHB luminosity.

The different sets of models were constructed following the same approach discussed in Marconi et al. (2015). The bolometric light curves were transformed into optical (*UBVRI*) and NIR (*JHK*)[11] bands using static atmosphere models (Bono et al. 1995a) and eventually intensity-weighted mean magnitudes and colors were computed. Preliminary results for interpreting Galactic Bulge RRLs were discussed in Marconi & Minniti (2018), while the details of these new helium-enriched models are presented in M. Marconi et al. (2018, in preparation).

[11] We adopted the 2MASS—JHK_s—photometric system.

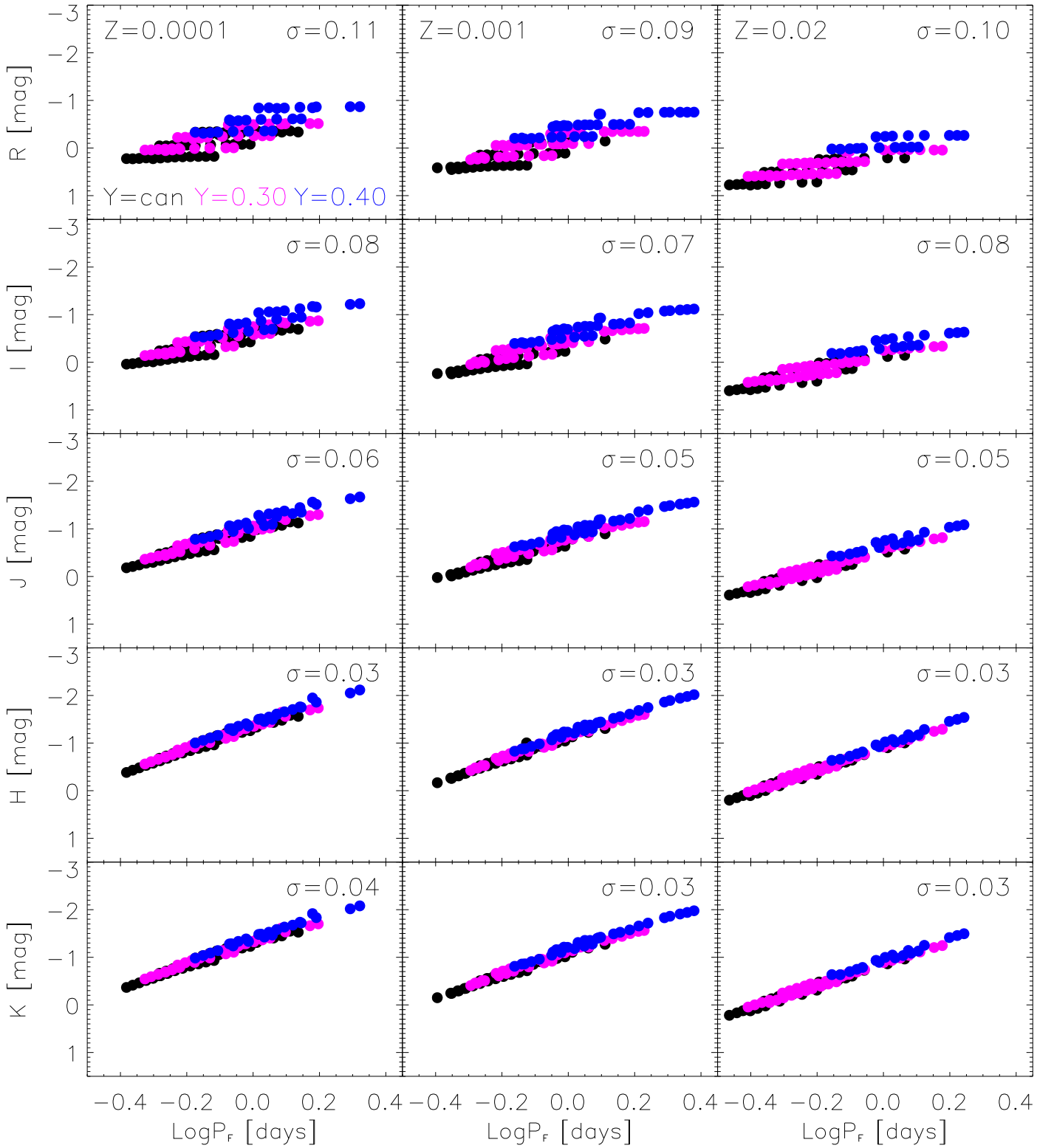

Figure 2. From top to bottom, predicted global (fundamental plus first overtone) PL relations in the *R*, *I*, *J*, *H*, *K* bands for three different metal abundances: $Z = 0.0001$ (left), $Z = 0.001$ (middle), and $Z = 0.02$ (right). Models plotted in each panel take into account different helium abundances: canonical *Y* as in Marconi et al. (2015; black), $Y = 0.30$ (magenta), and $Y = 0.40$ (blue). The standard deviations of the PL relations are labeled in the top right corner.

2.1. Predicted Optical/NIR PL Relations

Figure 2 shows the predicted optical/NIR PL distribution for five bands (*R*, *I*, *J*, *H*, *K*) and for three different metal abundances: $Z = 0.0001$ (left), $Z = 0.001$ (middle), and $Z = 0.02$ (right). In each panel, pulsation models constructed assuming a fixed helium-to-metal enrichment ratio (Marconi et al. 2015; black circles) are plotted together with models constructed assuming two different helium enhancements: $Y = 0.30$ (magenta circles) and $Y = 0.40$ (blue circles). Models plotted in this figure display two well defined trends

Table 1
Coefficients of the Predicted Global (Fundamental Plus First Overtone) Period–Luminosity–Metallicity–Helium (PLZY) Relations for RRLs in the Form $M_X = a + b \log P + c[\mathrm{Fe/H}] + d \log Y$, where X is the Selected Band

Band	a	b	c	d	σ
R	-0.63 ± 0.13	-1.30 ± 0.03	0.195 ± 0.007	-1.34 ± 0.07	0.13
I	-0.80 ± 0.11	-1.58 ± 0.03	0.190 ± 0.005	-1.10 ± 0.06	0.11
J	-1.00 ± 0.08	-1.92 ± 0.02	0.187 ± 0.004	-0.82 ± 0.04	0.08
H	-1.14 ± 0.06	-2.23 ± 0.02	0.188 ± 0.003	-0.55 ± 0.03	0.06
K	-1.16 ± 0.06	-2.26 ± 0.02	0.185 ± 0.003	-0.52 ± 0.03	0.06

among canonical and helium-enhanced models. (i) The period distribution of helium-enhanced models is systematically shifted toward longer periods when compared with canonical models. The difference is mainly caused by an evolutionary effect: a decrease in the mean stellar mass populating the RRL IS and an increase in the luminosity level (Marconi et al. 2011). (ii) The spread in luminosity between canonical and helium-enhanced models steadily decreases when moving from the *I*- to the *K*-band. The quoted spread is mainly caused by a difference in the zero-point, since the slopes are quite similar.

The plotted intensity-weighted *RIJHK* mean magnitudes can be used to predict multiband PL relations. The evolutionary and pulsation parameters of the helium-enhanced models will be provided in M. Marconi et al. (2018, in preparation) together with the bolometric mean magnitude and the transformation into different optical, NIR, and MIR photometric systems. Moreover, we plan to discuss the luminosity amplitudes for both canonical and He-enhanced models and their impact on the Bailey diagram. Finally, we plan to provide for the He-enhanced models the same distance diagnostics provided by Marconi et al. (2015). Table 1 gives the coefficients of the global[12] PL relations including both the metallicity and the helium terms ($M_X = a + b \log P + c[\mathrm{Fe/H}] + d \log \mathrm{Y}$, where X is the selected photometric band).

A glance at the coefficients listed in this table and to the models plotted in Figure 2 discloses three relevant features.

(i) The dependence on the period becomes, as expected, systematically steeper when moving from optical to NIR bands. This means that NIR PL relations are intrinsically more accurate than optical ones. The reason is twofold: (1) the standard deviation decreases by a factor of two when moving from the R/I to the H/K bands; (2) the coefficient of the metallicity term in the NIR bands attains similar values.

(ii) The helium dependence decreases by roughly 1 dex when moving from the *R* to the *K* band. This means that an increase in helium content causes, at fixed period and metal content, an increase in the *R* band of the order of a few tenths of a magnitude. The same increase causes a variation of the order of ≈0.05–0.08 mag in the NIR bands. Such an increase might introduce a mild systematic effect in distance determinations, but it appears negligible because it is similar to the standard deviations.

It has been suggested that the second stellar generation in GCs is made of materials that are enriched in helium, nitrogen, and sodium and depleted in carbon and oxygen. The enhancement in helium can be of the order of 0.05–0.10 (Renzini et al. 2015). However, there are reasons to believe that the quoted dependence of NIR PL relations on helium can be considered as a solid upper limit on the RRL distance scale. The reasons are as follows.

(i) The second stellar generation appears to be ubiquitous in GCs, but the current spectroscopic evidence indicates that they are very rare in the Galactic field (Gratton 2016). This means that only a few percent of the galactic stellar content might be helium enhanced.

(ii) He-enhanced stellar populations in the metal-poor and in the metal-intermediate regime cross the IS only during off-ZAHB evolution. This means that the evolutionary time spent inside the IS is at least one order of magnitude smaller compared with the canonical ones (see Section 2). Note that the He-enhanced ($Y = 0.30$) ZAHB crosses the IS in the metal-intermediate and in the metal-rich regime. This means that the probability of producing He-enhanced RRLs in the metal-poor regime is quite limited. Moreover, the crossing of the IS at brighter magnitudes (lower surface gravities) causes a systematic shift in the period distribution of He-enhanced RRLs toward longer periods. This also means that He-enhanced stellar populations are more prone to producing type II Cepheids ($P > 1$ day) than RRLs.

2.2. Mean Magnitude—M_B, M_V—Metallicity Relations

The visual mean magnitude metallicity (M_V–[Fe/H]) relation was foreseen by Baade (1958), and it was the most popular distance diagnostic for old stellar populations (Sandage 1990), but it is also prone to a number of potential systematic errors (Caputo et al. 2000; Bono et al. 2003; Di Criscienzo et al. 2004; Marconi et al. 2015).

We have already mentioned that an increase in He content causes, at fixed metallicity, an increase in stellar luminosity and, in turn, in the pulsation period. A glance at the predicted magnitudes plotted in the bottom panel of Figure 3 shows the impact of the He content. Canonical and He-enhanced models, as expected, partially overlap due to off-ZAHB evolution. However, He-enhanced models with $Y = 0.30$ (pink open circles) are on average ∼0.15 mag brighter than canonical ones, while those with $Y = 0.40$ (blue open circles) are almost a half-magnitude brighter.

The outcome is the same if we use the *B* band, but it should be cautiously treated for a possible color dependency (Catelan et al. 2004). Data plotted in the top panel of Figure 3 display that He-enhanced models are 0.2 ($Y = 0.30$) and 0.6 ($Y = 0.40$) mag systematically brighter than canonical ones. To investigate on a more quantitative basis the dependence of the mean magnitude metallicity (MZ) relations, we derived new

[12] This sample includes both fundamental and first overtone pulsators. The latter group was fundamentalized, i.e., $\log P_F = \log P_{FO} + 0.127$.

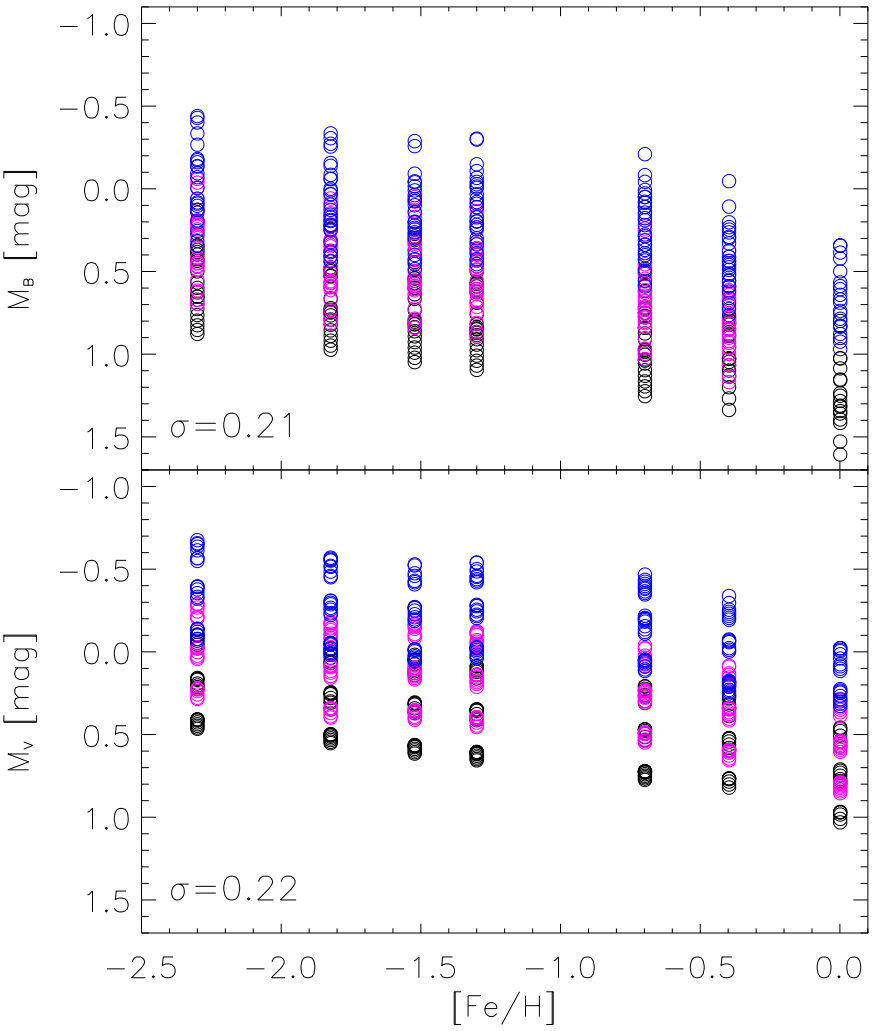

Figure 3. Top: predicted (fundamentals plus first overtones) B-band mean magnitude metallicity (M_B–[Fe/H]) relation. Symbols are the same as in Figure 2. The standard deviation is labeled in the bottom left corner. Bottom: same as the top, but for the M_V–[Fe/H] relation.

analytical relations including a He term (MZY), namely,

$$M_B(RR) = 0.28[\mathrm{Fe/H}] - 2.91 \log Y - 0.61$$

with an rms = 0.21 mag and

$$M_V(RR) = 0.22[\mathrm{Fe/H}] - 2.94 \log Y - 1.08$$

with an rms = 0.22 mag.

Data plotted in Figure 3 and the above MZY relations disclose a few relevant predictions concerning the possible occurrence of He-enhanced RRLs.

(i) Stellar systems hosting a sizable sample of RRLs covering a broad range in He abundance should show, at fixed metal content, a spread in visual and in B-band magnitudes that is on average a factor of two larger than canonical models. A detailed set of synthetic HB models is required to constrain the variation as function of both metal and He content. However, empirical evidence dating back to Sandage (1990) indicate that the spread in visual magnitude showed by cluster RRLs ranges from 0.2 mag in the metal-poor regime to 0.6 mag in the metal-intermediate regime. This trend was soundly confirmed by synthetic HB models by Bono et al. (1997).

(ii) Stellar systems hosting stellar populations with significantly different He contents should show multimodal magnitude distributions inside the IS. Indeed, He-enhanced models are characterized by ZAHBs that are systematically brighter. This difference in magnitude cannot be mixed up with a difference in metallicity, since the evolutionary lifetime of He-enhanced models inside the IS is, at fixed metal content, systematically shorter than canonical ones.

3. Final Remarks and Conclusions

We have presented new sets of He-enhanced ($Y = 0.30$, $Y = 0.40$) nonlinear, time-dependent convective hydrodynamical models of RRLs covering the same range of metal abundances investigated by Marconi et al. (2015). The model mean magnitudes in the *RIJHK* bands were used to obtain new period–luminosity–metallicity–helium relations in these filters (see Table 1). The main effect of an increase in He is an increase in the luminosity level and, in turn, in the predicted pulsation period. Therefore, an increase in primordial He content from the canonical value ($Y = 0.245$) to He-enhanced ($Y = 0.30$, 0.40) causes a minimal change in the coefficients of both period and metallicity terms, since the He-enhanced models obey similar PLZ relations. Owing to the sensitivity of the luminosity level to He variations, the classical relations connecting the B and V

mean magnitudes to metallicity and the *R*-band PLZ relation display a significant He dependence. The He-enhanced models models are, at fixed metallicity, 0.2 ÷ 0.5 mag brighter than canonical ones.

This is an interesting opportunity because *Gaia* is going to provide accurate geometrical distances to calibrate both the zero-point and the slopes of the diagnostics adopted to estimate individual RRL distances. Spectroscopic RRL abundances based on ground-based measurements (Magurno et al. 2018) will pave the way for an empirical calibration of the PLZ relations. This means the opportunity to determine distance, reddening, and chemical composition (metal, helium) for field RRLs that are simultaneously available for optical (*BVRI*) and NIR (*JHK*) mean magnitudes. Note that this approach applies to RRL in nearby stellar systems and, in turn, the opportunity to investigate the helium-to-metal enrichment ratio currently adopted in evolutionary and pulsation calculations is universal.

We thank our anonymous referees for the constructive comments. M.M. acknowledges partial support from Premiale 2015, "MITiC" (PI: B. Garilli).

ORCID iDs

M. Marconi https://orcid.org/0000-0002-1330-2927
G. Bono https://orcid.org/0000-0002-4896-8841
V. F. Braga https://orcid.org/0000-0001-7511-2830

References

Asplund, M., Grevesse, N., Sauval, A. J., & Scott, P. 2009, ARA&A, 47, 481
Baade, W. 1958, RA, 5, 165
Beaton, R. L., Freedman, W. L., Madore, B. F., et al. 2016, ApJ, 832, 210
Bono, G., Caputo, F., Cassisi, S., Castellani, V., & Marconi, M. 1997, ApJ, 479, 279
Bono, G., Caputo, F., Castellani, V., et al. 2003, MNRAS, 344, 1097
Bono, G., Caputo, F., Castellani, V., & Marconi, M. 1995a, ApJL, 448, L115
Bono, G., Caputo, F., Castellani, V., Marconi, M., & Storm, J. 2001, MNRAS, 326, 1183
Bono, G., Caputo, F., & Marconi, M. 1995b, AJ, 110, 2365
Braga, V. F., Dall'Ora, M., Bono, G., et al. 2015, ApJ, 799, 165
Cacciari, C., & Clementini, G. 2003, in Stellar Candles for the Extragalactic Distance Scale, ed. D. Alloin & W. Gieren (Berlin: Springer), 105
Caputo, F. 1998, A&ARv, 9, 33
Caputo, F., Castellani, V., Marconi, M., & Ripepi, V. 2000, MNRAS, 316, 819
Catelan, M., Pritzl, B. J., & Smith, H. A. 2004, ApJS, 154, 633
Chadid, M., Sneden, C., & Preston, G. W. 2017, ApJ, 835, 187
Coppola, G., Marconi, M., Stetson, P. B., et al. 2015, ApJ, 814, 71
Da Costa, G. S., Rejkuba, M., Jerjen, H., & Grebel, E. K. 2010, ApJL, 708, L121
Dall'Ora, M., Storm, J., Bono, G., et al. 2004, ApJ, 610, 269
D'Cruz, N. L., Dorman, B., Rood, R. T., & O'Connell, R. W. 1996, ApJ, 466, 359
Dékány, I., Hajdu, G., Grebel, E. K., et al. 2018, ApJ, 857, 54
Di Criscienzo, M., Marconi, M., & Caputo, F. 2004, ApJ, 612, 1092
Drake, A. J., Catelan, M., Djorgovski, S. G., et al. 2013, ApJ, 763, 32
Fiorentino, G., Contreras Ramos, R., Tolstoy, E., Clementini, G., & Saha, A. 2012, A&A, 539, A138
Fiorentino, G., Musella, I., & Marconi, M. 2013, MNRAS, 434, 2866
Gratton, R. G. 2016, in IAU Symp. 317, The General Assembly of Galaxy Halos: Structure, Origin and Evolution, ed. A. Bragaglia et al. (Cambridge: Cambridge Univ. Press), 259
Greggio, L., & Renzini, A. 1990, ApJ, 364, 35
Grevesse, N., Noels, A., & Sauval, A. J. 1993, A&A, 271, 587
Inno, L., Matsunaga, N., Bono, G., et al. 2013, ApJ, 764, 84
Longmore, A. J., Dixon, R., Skillen, I., Jameson, R. F., & Fernley, J. A. 1990, MNRAS, 247, 684
Madore, B. F. 1982, ApJ, 253, 575
Madore, B. F., Freedman, W. L., & Moak, S. 2017, ApJ, 842, 42
Magurno, D., Sneden, C., Braga, V. F., et al. 2018, arXiv:1807.06681
Marconi, M., Bono, G., Caputo, F., et al. 2011, ApJ, 738, 111
Marconi, M., Coppola, G., Bono, G., et al. 2015, ApJ, 808, 50
Marconi, M., & Minniti, D. 2018, ApJL, 853, L20
Monelli, M., Fiorentino, G., Bernard, E. J., et al. 2017, ApJ, 842, 60
Neeley, J. R., Marengo, M., Bono, G., et al. 2017, ApJ, 841, 84
Pietrinferni, A., Cassisi, S., Salaris, M., & Castelli, F. 2006, ApJ, 642, 797
Pietrukowicz, P., Kozłowski, S., Skowron, J., et al. 2015, ApJ, 811, 113
Renzini, A., D'Antona, F., Cassisi, S., et al. 2015, MNRAS, 454, 4197
Riess, A. G., Macri, L., Casertano, S., et al. 2012, ApJ, 752, 76
Ripepi, V., Moretti, M. I., Marconi, M., et al. 2012, MNRAS, 424, 1807
Sandage, A. 1990, ApJ, 350, 603
Sarajedini, A., Yang, S.-C., Monachesi, A., Lauer, T. R., & Trager, S. C. 2012, MNRAS, 425, 1459
Sollima, A., Borissova, J., Catelan, M., et al. 2006, ApJL, 640, L43
Soszyński, I., Udalski, A., Szymański, M. K., et al. 2010, AcA, 60, 165
Soszyński, I., Udalski, A., Szymański, M. K., et al. 2014, AcA, 64, 177
Valcarce, A. A. R., Catelan, M., & Sweigart, A. V. 2012, A&A, 547, A5
Vivas, A. K., & Zinn, R. 2006, AJ, 132, 714
Walker, A. R., & Terndrup, D. M. 1991, ApJ, 378, 119
Zinn, R., Horowitz, B., Vivas, A. K., et al. 2014, ApJ, 781, 22